

Soil moisture estimation in a semiarid rangeland using ERS-2 and TM imagery

Cuizhen Wang^{a,*}, Jiaguo Qi^a, Susan Moran^b, Robin Marsett^b

^a Centre for Global Change and Earth Observations and Department of Geography, Michigan State University, 101 Manly Miles Building, 1405 South Harrison Road, East Lansing, MI 48823, USA

^b USDA-ARS Southwest Watershed Research Centre, 2000 E. Allen Rd., Tucson, AZ 85719, USA

Received 23 June 2003; received in revised form 3 December 2003; accepted 6 December 2003

Abstract

Soil moisture is important information in semiarid rangelands where vegetation growth is heavily dependent on the water availability. Although many studies have been conducted to estimate moisture in bare soil fields with Synthetic Aperture Radar (SAR) imagery, little success has been achieved in vegetated areas. The purpose of this study is to extract soil moisture in sparsely to moderately vegetated rangeland surfaces with ERS-2/TM synergy. We developed an approach to first reduce the surface roughness effect by using the temporal differential backscatter coefficient ($\Delta\sigma_{\text{wet-dry}}^0$). Then an optical/microwave synergistic model was built to simulate the relationship among soil moisture, Normalized Difference Vegetation Index (NDVI) and $\Delta\sigma_{\text{wet-dry}}^0$. With NDVI calculated from TM imagery in wet seasons and $\Delta\sigma_{\text{wet-dry}}^0$ from ERS-2 imagery in wet and dry seasons, we derived the soil moisture maps over desert grass and shrub areas in wet seasons. The results showed that in the semiarid rangeland, radar backscatter was positively correlated to NDVI when soil was dry ($m_v < 10\%$), and negatively correlated to NDVI when soil moisture was higher ($m_v > 10\%$). The approach developed in this study is valid for sparse to moderate vegetated areas. When the vegetation density is higher ($\text{NDVI} > 0.45$), the SAR backscatter is mainly from vegetation layer and therefore the soil moisture estimation is not possible in this study.

© 2004 Elsevier Inc. All rights reserved.

Keywords: Soil moisture; TM imagery; ERS-2 imagery

1. Introduction

Microwave remote sensing is sensitive to soil moisture because its dielectric constant, which is mainly related to moisture, is one of the most important factors in radar backscatter intensity. However, radar backscatter is not linearly related to soil moisture. It is also influenced greatly by soil roughness, vegetation amount, structure, and system parameters such as incidence angle and frequency. Sano et al. (1998a) reported that the sensitivity of Synthetic Aperture Radar (SAR) data to soil moisture varied significantly at different roughness scales. Depending on the frequency and incidence angle, radar backscatter coefficients (σ^0) could vary up to 22 dB due to surface roughness variation (Ulaby et al., 1978). The changes in σ^0 due to the variation in vegetation cover could be as high as 15 dB (Dobson & Ulaby, 1986). SAR imagery acquired with steeper incidence

angles is less affected by roughness and vegetation (Schmullius & Evans, 1997). P-band (68-cm wavelength) backscatter is less affected by vegetation geometry, but the attenuation of canopy in C-band (5.8 cm) may be too strong to monitor soil moisture with monotemporal data (Wever & Henkel, 1995).

A number of models have been developed to map soil moisture distribution with SAR data. Most models utilized multipolarization features and have been applied primarily to bare soil fields (Dubois et al., 1995; Oh et al., 1992; Shi et al., 1997). The success of these modeling approaches is primarily due to the capability of longer wavelengths and multiple polarizations of the data with which the roughness effect is less dominant (Chen et al., 1995). However, these data could only be acquired from the sensors on space shuttles, airplanes or trucks that are limited in space and time (Sano et al., 1998b). The widely available SAR data from spaceborne sensors like ERS (C-VV) and JERS (L-HH) are single frequency and single polarization, and therefore cannot be applied in these models. Moreover,

* Corresponding author. Tel.: +1-5174324765; fax: +1-5173532932.
E-mail address: wanguizhen@msu.edu (C. Wang).

the accuracy of these models is significantly reduced when applied to vegetated surfaces (Taconet et al., 1996). Because most areas where the water availability is of great importance are covered by vegetation, the use of the satellite data in soil moisture estimation is thus limited. Using multi-temporal ERS data in wintertime when the vegetation effect was minimal, Verhoest et al. (1998) examined the surface “wetness” pattern by relating the surface drainage information to the second principal component in a principal component analysis. However, because this component only accounted for 6.6% of the total variance, it was difficult to quantify the soil moisture when the surface roughness effect was not considered.

One of the main challenges in soil moisture estimation using the single-frequency, single-polarization SAR data is to remove/reduce surface roughness effect. In studies over small areas, the roughness condition [root mean square (rms) height and correlation length (cl)] could be approximated with intense ground measurements and simulations. However, it is too time consuming to be applied over large areas. In most soil moisture estimation models, surface roughness is characterized by autocorrelation functions for the surface profile (Ulaby et al., 1982). Over large areas, a single function is often too simple to fully represent the surface roughness conditions. In areas such as semiarid rangelands where roughness changes little with time, the difference of multitemporal SAR data may provide ways to reduce the roughness effect.

Another challenge in soil moisture estimation is to reduce the effect of vegetation atop a soil surface. Although radar signals may penetrate vegetation, the interpretation of surface backscatter is often difficult because of the interactions between vegetation and underlying soils. Optical remote sensing has been widely used to derive information of vegetation properties such as fractional cover and green leaf area index (Jasinski & Eagleson, 1990; Qi et al., 2000). The Normalized Difference Vegetation Index (NDVI) is almost linearly related to vegetation abundance at lower density (Qi et al., 1994) and therefore, can represent the vegetation effect in soil moisture estimation.

The objective of this study is to investigate the feasibility of estimating soil moisture by synergistic use of multi-temporal ERS-2 and TM images. In this study, an optical/microwave synergistic model was built and the relationships between soil moisture, roughness, and NDVI were simulated. The model was then applied to map soil moisture distribution in sparsely to moderately vegetated semiarid rangelands.

2. Study area and data set

The experimental area of this study is in the San Pedro River basin in southeast Arizona, USA. Due to the limitation of image acquisition, only a subset of the basin nearby Tombstone is selected, covering an area of approximately

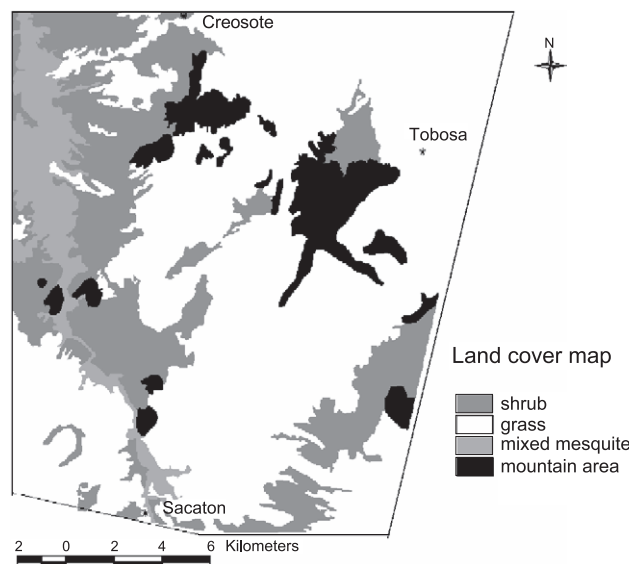


Fig. 1. Land cover map of the study area. Three study sites: Creosote, Tobosa, and Sacaton are labeled in the map.

400 km². A land cover map (Fig. 1) of the study area was made with supervised classification techniques over an ETM+ image acquired in September 1999. The accuracy of classification was around 90% (Wallace et al., 2003). The dominant vegetation types in the study area are long-leaf desert grasses, small elliptic-leaf desert shrubs, and mesquites mixed with cottonwood along the San Pedro River. The dense vegetation cover of mixed mesquites attenuates SAR signals and, therefore, highly reduces the backscatter intensity from underneath soils. Only grass and shrub areas were used in this study.

Three study sites were selected and each site was characterized primarily by one of the three vegetation types: Sacaton (*Sporobolus wrightii*), Creosote (*Larrea tridentata*), and Tobosa (*Hilaria mutica*). Both Sacaton and Tobosa belong to desert grass, while Creosote is typical desert shrub. Each study site had an area of 90 × 90 m. The GPS readings in the center of the site were recorded during fieldwork. In situ soil moisture measurements were made on days when ERS-2 overpassed (Table 1). Within each study site, a 6 × 6 grid was laid out with an interval of 15 m in both *x* and *y* directions. At each time of the overpass, one soil sample was collected at each corner of the grids. The soil moisture at this study site was statistically represented by these 49 (7 × 7) samples.

Fine sandy loam (often with gravel or cobbles) is the predominant soil texture in this area. Except some isolated mountain areas, the study area is mostly composed of fan terraces mixed with fan alluvium of 0–15% slopes (Soil Survey, 1996). Therefore, the topographical effect on radar backscatter is not accounted for in this study. The average surface soil roughness is 0.53 ± 0.15 in grass dominant sites and 0.55 ± 0.23 in shrub dominant areas (Moran et al., 2000).

Table 1

In situ soil moisture measurements at the study sites (Moran et al., 2001)

Date	DOY (day of year)	Volumetric soil moisture			Notes
		Sacaton	Creosote	Tobosa	
01/12/97	012 (winter wet)	28.2 ± 5.1	9.0 ± 1.4	19.3 ± 6.1	It snowed in early January, and the snow had melted by the time of the ERS-2 overpass.
03/23/97	082 (spring dry)	7.3 ± 4.3	1.1 ± 0.8	3.7 ± 1.1	There was minimal rain in March, and the soil conditions were moderately dry.
07/06/97	187 (end of spring dry)	3.1 ± 1.1	0.7 ± 0.2	2.2 ± 0.6	During the hot months of May and June, the soil at all sites was very dry.
09/14/97	257 (summer monsoon)	13.8 ± 5.0	3.8 ± 1.1	7.0 ± 2.6	A small storm preceded the September overpass.

The climate seasonal characteristics in the San Pedro River basin include a summer monsoon season from early July to mid-September, a fall dry season from mid-September to mid-December, a winter wet season from mid-December to March, and a spring dry season from April to June. Approximately 25% of the annual precipitation occurs in the winter as widespread snow or soaking rains, while 75% of the precipitation is in the summer as isolated, short duration, heavy thunderstorms.

In this study, four pairs of ERS-2/TM data were acquired in three seasons in 1997 (Fig. 2). The first pair, ERS-2 (DOY187)/TM (DOY191), was acquired at the end of spring dry season. The second pair, ERS-2 (DOY257)/TM (DOY255), was in summer monsoon season. The third pair, ERS-2 (DOY012)/TM (DOY015), was in winter wet season, and the fourth pair, ERS-2 (DOY082)/TM (DOY079) was in spring dry season. These four pairs of data formed two wet–dry data sets: DOY257–DOY187 and DOY012–DOY082. The duration of each wet–dry data set was less than 3 months and therefore, the change of soil roughness

and vegetation structure between wet and dry seasons was assumed minimal.

For each image pair, the TM image was geometrically corrected with ground control points, and the ERS-2 image was georeferenced to TM. The cloud/shadow and isolated mountain areas in each pair were masked out in the analysis. The atmospheric effect on TM images was corrected using a refined empirical line approach (Moran et al., 2001). The backscatter coefficient (σ^0) of ERS-2 images was calculated with the equations from the European Space Agency.

3. Approach

In this study, we first build an optical/microwave synergistic model to simulate radar backscatter from a vegetated surface. Second, the ratio of backscatter in wet and dry soil surfaces is calculated to reduce the roughness effect. Third, the temporal differential backscatter coefficient ($\Delta\sigma_{\text{wet-dry}}^0$) is modeled as a function of NDVI with random soil roughness

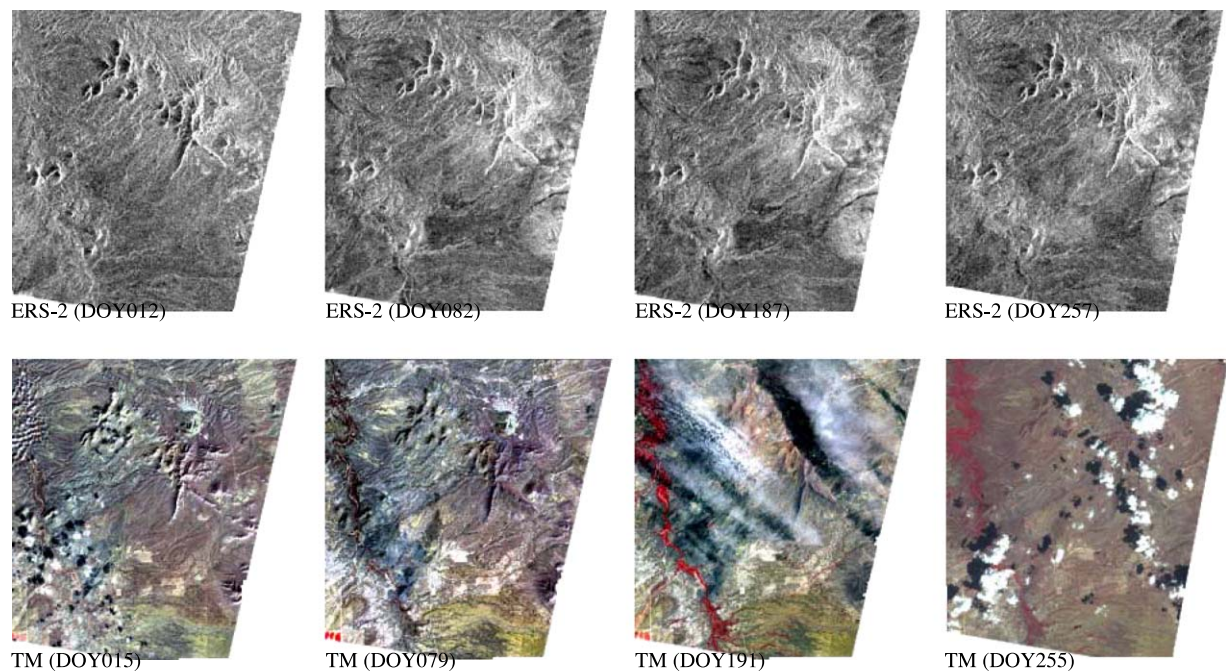


Fig. 2. Paired ERS-2/TM images of the study area in three seasons in 1997: winter wet, spring dry, end of spring dry, and summer monsoon.

values to examine the vegetation effect. The relationships among soil moisture, NDVI, and $\Delta\sigma_{\text{wet-dry}}^0$ are also examined using the model simulation. Finally, the NDVI from TM in wet seasons and $\Delta\sigma_{\text{wet-dry}}^0$ from ERS-2 in wet and dry seasons are used to establish a series of isomoisture lines and then to map soil moisture distributions in wet seasons.

3.1. An optical/microwave synergistic model

In desert grass areas, the radar backscatter results primarily from leaf canopy and underneath soil. In shrub areas, the radar backscatter results from leaf canopy, stem/branch, and underneath soil. However, it is assumed that the stem/branch contribution remains less dominant because they are similarly dry in wet and dry seasons. When $\Delta\sigma_{\text{wet-dry}}^0$ in wet and dry seasons is used, the stem/branch contribution in total backscatter is assumed to cancel out in the first-order radiative transfer solution. It is also assumed that the moisture of the leaves of desert grass and shrub is constantly high in wet seasons and low in dry seasons. Under these assumptions, both grass and shrub areas in wet season can be modeled as a single homogeneous canopy layer atop a soil surface. The canopy layer is composed of small elliptic scatters characterized by their orientation probability distribution functions (Table 2). The scatters of each vegetation type have constant dielectric characteristics, size, orientation probability distribution, and layer height. The soil underneath is modeled as a continuous surface on which the radar backscatter is determined primarily by soil roughness and moisture. The surface in dry season is assumed to be bare surface.

Table 2
Input parameters of the optical/microwave synergistic model

General parameters		
Wavelength (cm)	5.3	
Incidence zenith angle (°)	23	
Incidence azimuth angle (°)	0–360	
Vegetation parameters	Grass	Shrub
Total number of layers	1	1
Total number of leaf groups/layer	1	1
Leaf longer semiaxis (cm)	10	0.7
Leaf shorter semiaxis (cm)	1	0.6
Leaf depth (cm)	0.05	0.05
Leaf dielectric constant	15.4–9.5i	15.4–9.5i
Layer height (cm)	30	50
Leaf PDF function	$\sin 2\theta$	$2(1 + \cos 2\theta)/\pi$
NDVI series for modeling	0.1 (bare), 0.15, 0.2, 0.3, 0.4, 0.5, 0.6	
Soil surface parameters	100 points in	100 points in
rms height series for modeling (cm)	(0.38, 0.68)	(0.32, 0.78)
Soil moisture series for modeling (%)	1, 5, 10, 15, 20, 25, 30, 35, 40	

The microwave canopy scattering model developed by Karam et al. (1992) divides the radar backscatter on the vegetated surface into three parts: volume scattering from leaf canopy σ_{leaf} , double bounce between vegetation ground σ_{doubleb} , and direct soil surface backscatter σ_{soil} . The intensity of double bounce from desert grass and shrub canopy is much lower than other scattering. The model can be written as (in power unit):

$$\sigma = \sigma_{\text{leaf}} + \sigma_{\text{doubleb}} + \tau^2 \sigma_{\text{soil}} \quad (1)$$

where τ is the attenuation factor in either forward or backward direction:

$$\tau = e^{-kH/\cos\theta} \quad (2)$$

where H is the canopy height. The extinction coefficient (k) is the total extinction cross section of all leaves statistically averaged over the leaf orientation probability distribution. For VV polarization,

$$k = \frac{4\pi N}{k_0} \text{Im}\langle F_{\text{vv}} \rangle \quad (3)$$

where k_0 is the wave number. F_{vv} is the VV component of the scattering matrix, or scattering amplitude tensor, of a single leaf. N is the leaf number density (No./m³).

Two modifications to Karam et al.'s (1992) model are made in this study. The first one is to introduce an IEM bare surface scattering model into Karam et al.'s (1992) canopy scattering model. The second one is to link the model to optical remote sensing variables.

In Karam et al.'s (1992) model, the σ_{soil} in Eq. (1) is a very simplified first-order solution of radiative transfer equations, assuming the soil as a continuous and slightly rough dielectric surface. It is thus insufficient to simulate radar backscatter under various soil roughness and moisture conditions. An IEM model developed especially for bare surface scattering with a wide range of roughness and wetness (Fung et al., 1992) is used to replace the σ_{soil} in Karam et al.'s (1992) model. This replacement would allow more realistic soil moisture contribution in total backscatter of Eq. (1).

Let a and b be the half-length and half-width of an elliptic leaf, respectively, the leaf density number N in Eq. (3) can be related to the leaf area index (LAI) by:

$$N = \frac{\text{LAI}}{\pi abH} \quad (4)$$

In semiarid rangelands, the LAI can be estimated from NDVI that is derived from optical remote sensing data like TM imagery (Qi et al., 2000):

$$\text{LAI} = 18.99\text{NDVI}^3 - 15.24\text{NDVI}^2 + 6.124\text{NDVI} - 0.352 \quad (5)$$

By replacing the simple soil scattering model with the IEM model and linking some vegetation parameters to optical data, an optical/microwave synergistic model is then devel-

oped to simulate scattering from vegetated surfaces. The input parameters of this model are listed in Table 2. Only VV backscatter in C-band with incidence angle 23° is modeled in consistence with ERS-2 configuration.

3.2. Roughness reduction

Combining σ_{leaf} and σ_{doubleb} as σ_{veg} , Eq. (1) becomes:

$$\begin{aligned}\sigma_{\text{wet}} &= \sigma_{\text{veg}} + \tau^2 \sigma_{\text{soil_wet}} \\ \sigma_{\text{dry}} &= \sigma_{\text{soil_dry}}\end{aligned}\quad (6)$$

In the IEM model, except for very smooth or very rough surface conditions, the first-order backscatter due to roughness and volumetric soil moisture content (m_v) are approximately multiplicative (Fung et al., 1992). Assuming that the soil surface in dry season is constantly dry, the soil backscatter in wet and dry seasons can be described as (in power unit):

$$\begin{aligned}\sigma_{\text{soil_wet}} &= f_1(\text{roughness})f_2(m_v) \\ \sigma_{\text{soil_dry}} &= f_1(\text{roughness}) \cdot C\end{aligned}\quad (7)$$

where $f_1(\text{roughness})$ and $f_2(m_v)$ are functions of roughness and moisture, respectively. C is related to the soil moisture that is assumed to be constant in dry season. The ratio of total backscatter in Eq. (6) then becomes:

$$\frac{\sigma_{\text{wet}}}{\sigma_{\text{dry}}} = \tau^2 f_2(m_v) + \frac{\sigma_{\text{veg}}}{f(\text{roughness})}\quad (8)$$

From Eqs. (2)–(6), the attenuation factor τ is a function of NDVI from optical data in wet season. For sparse vegetation in rangelands, the second term in Eq. (8) is small. When vegetation density is higher, σ_{veg} is higher. For smooth to medium rough surfaces such as semiarid rangelands, $f_1(\text{roughness})$ has a range of variation which makes the second term in Eq. (8) small but unable to be determined. It can be treated as an error term ε . Then Eq. (8) can be rewritten as (in power unit):

$$\frac{\sigma_{\text{wet}}}{\sigma_{\text{dry}}} = f(m_v)g(\text{NDVI}) + \varepsilon\quad (9)$$

The error term ε changes with the variation in vegetation and soil roughness. Define $\varepsilon\%$ as the ratio of ε to the differential backscatter $\sigma_{\text{wet}}/\sigma_{\text{dry}}$, the magnitude of ε in Eq. (9) is examined with various NDVI, soil moisture m_v , and roughness values (Fig. 3). The value of ε is around 5% for sparse vegetation and 30% for dense vegetation atop soil surfaces with medium roughness and moisture conditions. The magnitude of ε is lower when soil is rougher (Fig. 3a) or soil moisture is higher (Fig. 3b). Fig. 3 indicates that the differential approach is valid for vegetated surfaces with low to medium vegetation cover. When vegetation is denser (e.g., $\text{NDVI} > 0.5$), the ε is dominant and Eq. (9) is no longer valid.

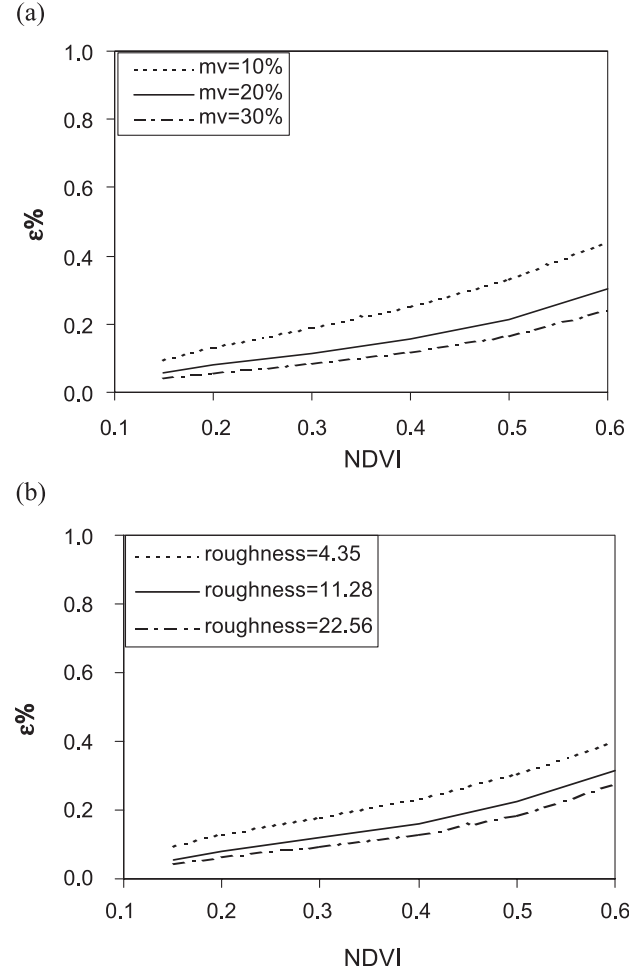


Fig. 3. Sensitivity of $\varepsilon\%$ to roughness (a) and m_v (b) with the variation in NDVI.

Define the dB value of $\sigma_{\text{wet}}/\sigma_{\text{dry}}$ as differential backscatter coefficient $\Delta\sigma_{\text{wet-dry}}^0$, Eq. (9) can be rewritten as (in dB value):

$$\Delta\sigma_{\text{wet-dry}}^0 \cong f'(m_v) + g'(\text{NDVI}) + \varepsilon'\quad (10)$$

Here both m_v and NDVI is in wet season. Eq. (10) indicates that $\Delta\sigma_{\text{wet-dry}}^0$ is contributed additively from soil moisture and vegetation properties. The error term ε' in Eq. (10) is related to ε in Eq. (9) which accounts for the variation in vegetation and soil roughness. Because ε' is much less dominant than the other two terms, the roughness effect has been effectively reduced in this model.

The model is tested with paired TM/ERS-2 images and ground measurements at three study sites (Fig. 4). One $\Delta\sigma_{\text{wet-dry}}^0$ set is modeled with soil moisture measured in both wet and dry seasons. Another $\Delta\sigma_{\text{wet-dry}}^0$ set is derived from ERS-2 images. NDVI is retrieved from TM images in wet seasons. The soil moisture of Creosote in dry season (1.1% in DOY082 and 0.7% in DOY187) is replaced by 3% (the average of the soil moisture measurements in dry season) because the modeled backscatter with such low

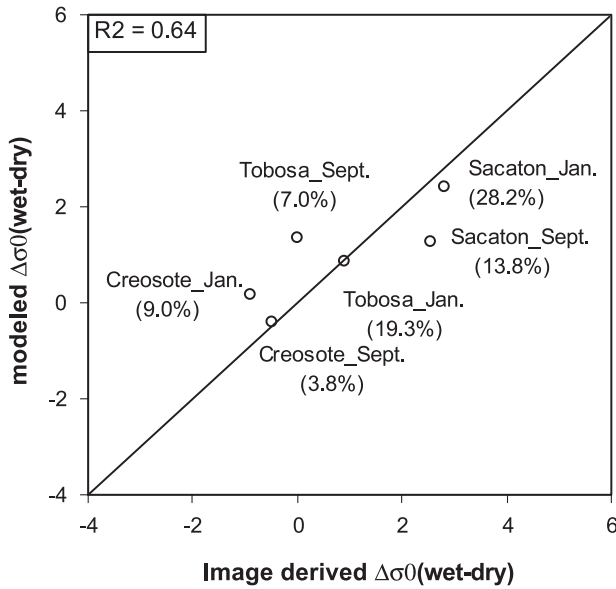


Fig. 4. Scatterplot of modeled and image derived $\Delta\sigma_{\text{wet-dry}}^0$ in two wet seasons (summer monsoon and winter wet) at three study sites. The 1:1 line is labeled on the plot.

moisture is unreasonably low. In the scatterplot of the modeled and image-derived $\Delta\sigma_{\text{wet-dry}}^0$ in Fig. 4, all points are distributed along the 1:1 line. The modeled $\Delta\sigma_{\text{wet-dry}}^0$ is highly correlated to image derived $\Delta\sigma_{\text{wet-dry}}^0$ with $R^2 = 0.64$.

The feasibility of the differential approach to reduce roughness effect is also tested by examining the sensitivity of image derived σ^0 and $\Delta\sigma_{\text{wet-dry}}^0$ to ground measured soil moisture. To be scaling comparable, both σ^0 and $\Delta\sigma_{\text{wet-dry}}^0$ are normalized to (0,1). The relationship between normalized σ^0 (and $\Delta\sigma_{\text{wet-dry}}^0$) and m_v at three study sites in two wet seasons is shown in Fig. 5. It is obvious that before the subtraction, the correlation between σ^0 and m_v is very weak. One of the primary reasons is the soil roughness effect.

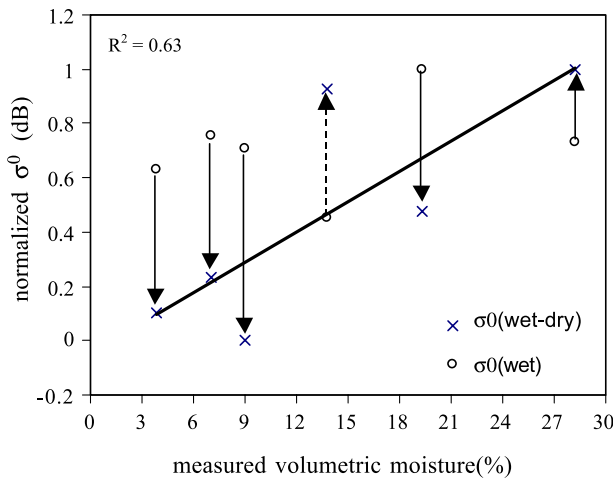


Fig. 5. Normalized σ^0 ($\Delta\sigma_{\text{wet-dry}}^0$)– m_v relationships before and after roughness reduction at three study sites in summer monsoon and winter wet seasons. The σ^0 and $\Delta\sigma_{\text{wet-dry}}^0$ are normalized to (0,1) for the scaling effect.

When the subtraction is applied, $\Delta\sigma_{\text{wet-dry}}^0$ correlates well with soil moisture ($R^2 = 0.63$) and most data points move closer to the correlation line, indicating that the roughness effect has been reduced. Among three sites in two wet seasons, only the Sacaton site in summer monsoon season ($m_v = 13.8\%$) is controversial, at which $\Delta\sigma_{\text{wet-dry}}^0$ is moving away from the correlation line. This will be explained later.

3.3. $\Delta\sigma_{\text{wet-dry}}^0$ –NDVI relationships

The $\Delta\sigma_{\text{wet-dry}}^0$ –NDVI relationships described in Eq. (10) are explored with model simulation and image observations. Fig. 6a is a scatterplot of $\Delta\sigma_{\text{wet-dry}}^0 \sim \text{NDVI}$ observed in ERS-2 and TM imagery in summer monsoon season (DOY257). The $\Delta\sigma_{257-187}^0$ image is geocorrected and resampled to the same pixel size (28.5 m) as TM (DOY255) to ensure that pixels from both images correspond to the same locations on the ground. The data points are randomly

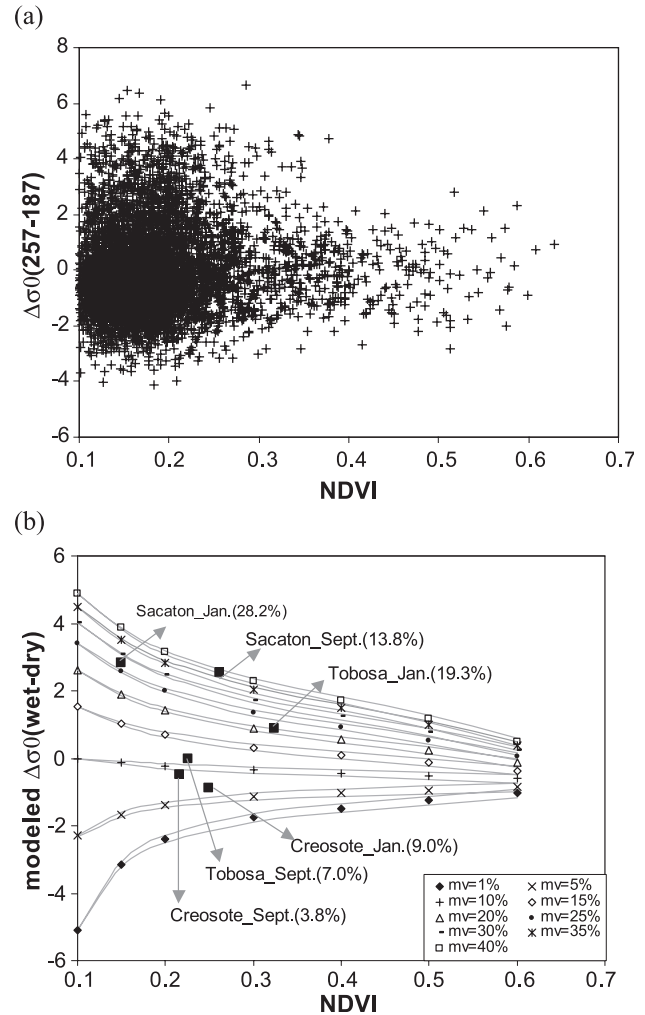


Fig. 6. Scatterplots of observed (a) and modeled (b) $\Delta\sigma_{\text{wet-dry}}^0$ –NDVI in grass and shrub areas in summer monsoon season. The 95% upper and lower confidence levels and six ground-measured points in three sites in two wet seasons are shown in (b).

selected in grass and shrub areas. A 3×3 moving window is used to reduce autocorrelation and speckle effects in ERS-2 images. To avoid cloud/shadow and other ground conditions (such as water bodies and buildings), data points with $\text{NDVI} < 0.1$ are not used in this plot. Fig. 6a suggests two trends of the relationships that $\Delta\sigma_{257-187}^0$ is either positively or negatively related to NDVI. The value of $\Delta\sigma_{257-187}^0$ is higher than 0 dB in the positive trend and lower than 0 dB in the negative trend.

The $\Delta\sigma_{\text{wet-dry}}^0$ -NDVI relationships are also simulated using the optical/microwave synergistic model in grass and shrub areas. For either grass or shrub, the general parameters and most of the vegetation parameters do not change (Table 2). NDVI has 7 values from 0.1 to 0.6. Soil moisture has 9 values from 1% to 40%. One hundred (100) soil root mean square (rms) height values are randomly selected in the range of (0.38, 0.68) with a mean of 0.53 for grass, and in the range of (0.32, 0.78) with a mean of 0.55 for shrub areas. Soil correlation length (cl) is calculated assuming rms slope $\sqrt{2} \cdot \text{rms}/\text{cl} = 0.1$. Each symbol in Fig. 6b is a modeled $\Delta\sigma_{\text{wet-dry}}^0$ value with one NDVI and soil moisture averaged over 100 roughness conditions. The modeled $\Delta\sigma_{\text{wet-dry}}^0$ -NDVI confirms the trends shown in Fig. 6a. The symbols form nine isomoisture series. The 95% upper and lower confidence levels for each series are also drawn in Fig. 6b.

In this differential approach, the soil moisture in dry season is assumed to be constant. Choosing a different value of this constant affects the $\Delta\sigma_{\text{wet-dry}}^0$ values but not the shape in Fig. 6b and consequently the soil moisture distribution in wet season. In this study, a value of 10% is assumed to be the soil moisture in dry season. The $\Delta\sigma_{\text{wet-dry}}^0$ values of $m_v = 1\%$ and $m_v = 5\%$ isomoisture lines are less than 0 dB because their soil moisture values are less than 10%. This agrees with the lower part of Fig. 6a. Because the soil moisture in summer monsoon season depends on the isolated precipitation, there may have some areas with lower soil moisture than in dry season. Therefore, The $\Delta\sigma_{\text{wet-dry}}^0$ values are less than 0 dB in these areas.

The $\Delta\sigma_{\text{wet-dry}}^0$ -NDVI trends in Fig. 6 are the result of different contribution from vegetation and soil underneath. Dobson and Ulaby (1998) reported that, from a nonflooded soil surface, marsh grass was primarily an attenuator of the radar backscatter. The σ^0 values decreased with the increasing biomass, even when the volumetric soil moisture was as low as 10%. Only in the flooded area would σ^0 increase with biomass. These results are consistent with the upper trend in Fig. 6 where $\Delta\sigma_{\text{wet-dry}}^0$ decreases with the increase of NDVI. For the lower trend in the plot, however, our data show an increase in backscatter with increasing NDVI under non-flooded conditions. It was found by Wang et al. (1994) that when biomass was less than 1.0 kg/m^2 , as the surface soil moisture decreased, the major contribution changed from soil surface backscatter to canopy volume scatter. It indicates that even under the situation of low vegetation density, when soil surface is dry, the primary contributor is canopy and,

therefore, backscatter will increase with increasing NDVI. This is consistent with the lower trend in Fig. 6.

As discussed earlier, soil roughness effect is reduced when differential backscatter coefficient $\Delta\sigma_{\text{wet-dry}}^0$ is applied. The variation of backscatter in Fig. 6 is thus primarily due to the vegetation abundance and soil moisture. When $\Delta\sigma_{\text{wet-dry}}^0$ is negatively correlated to NDVI, soil moisture is high and has dominant contribution to the radar backscatter. In this case, at a given soil moisture value, the increase in $\Delta\sigma_{\text{wet-dry}}^0$ due to increasing vegetation does not compensate for the soil backscatter decrease due to attenuation. Therefore, $\Delta\sigma_{\text{wet-dry}}^0$ decreases with increasing NDVI. In contrast, when $\Delta\sigma_{\text{wet-dry}}^0$ is positively correlated to NDVI, soil is dry and vegetation is the dominant contributor. Consequently, $\Delta\sigma_{\text{wet-dry}}^0$ increases with increasing NDVI. For data points in the center of the plot (around $\Delta\sigma_{\text{wet-dry}}^0 = 0$), when NDVI increases, the decrease in soil backscatter due to attenuation is compensated by the increase of vegetation backscatter. Thus, there is little change in $\Delta\sigma_{\text{wet-dry}}^0$ when NDVI increases.

3.4. Isomoisture lines

For each NDVI in Fig. 6, the vertical variation in $\Delta\sigma_{\text{wet-dry}}^0$ is mainly due to soil moisture. The vertical variation decreases as NDVI increases because the attenuation by vegetation is higher, indicating that the sensitivity of SAR backscatter to soil moisture decreases with increasing NDVI. Moran et al. (1997) found that SAR backscatter was sensitive to soil moisture in cotton fields only when $\text{NDVI} < 0.45$. It is also shown in Fig. 6 that when NDVI is higher, the $\Delta\sigma_{\text{wet-dry}}^0$ -NDVI relationships become saturated. The 95% confidence levels in Fig. 6b overlap when $\text{NDVI} > 0.45$. Most of the NDVI values of desert grass and shrub are around 0.1–0.3. Only very few pixels can reach 0.45 or higher in the study area. The mixed mesquite areas have much higher NDVI values and therefore are not included in this study.

As shown in Fig. 6b, for each soil m_v value, there is one $\Delta\sigma_{\text{wet-dry}}^0$ -NDVI isomoisture line. The $\Delta\sigma_{\text{wet-dry}}^0$ -NDVI trend is positive when $m_v < 10\%$ and negative when $m_v > 10\%$. When soil moisture is around 10%, there is little change in $\Delta\sigma_{\text{wet-dry}}^0$ when NDVI increases. It also shows that when NDVI is higher, due to the increasing vegetation backscatter, the variation of $\Delta\sigma_{\text{wet-dry}}^0$ in each isomoisture line is higher and the distance between upper and lower 95% confidence levels is longer. This is consistent with the error ε in Eq. (9). When vegetation density is high, the ε due to the vegetation backscatter becomes high. When NDVI is higher than 0.45, the isomoisture lines are too close to each other. This approach is no longer valid.

A rangeland surface with 5% soil moisture or lower is very dry and has little green vegetation. In fact, most of the rangeland surfaces in wet season should have soil moisture higher than 5%. In contrast, the surface with 30% soil moisture or higher is wet and provides adequate water for

vegetation growth. A series of soil moisture equations in the study area are regressed from the modeled $\Delta\sigma_{\text{wet-dry}}^0$ –NDVI results (all regressions have R^2 larger than 0.96).

$$m_v \leq 5\% : \Delta\sigma_{\text{wet-dry}}^0 \leq 36.59\text{NDVI}^3 - 46.84\text{NDVI}^2 + 19.87\text{NDVI} - 3.80$$

$$5\% < m_v \leq 10\% : \Delta\sigma_{\text{wet-dry}}^0 \leq -1.14\text{NDVI} + 0.04$$

$$10\% < m_v \leq 15\% : \Delta\sigma_{\text{wet-dry}}^0 \leq 7.57\text{NDVI}^2 - 8.75\text{NDVI} + 2.23$$

$$15\% < m_v \leq 20\% : \Delta\sigma_{\text{wet-dry}}^0 \leq -1.47\log(\text{NDVI}) - 0.85$$

$$20\% < m_v \leq 25\% : \Delta\sigma_{\text{wet-dry}}^0 \leq -1.79\log(\text{NDVI}) - 0.79$$

$$25\% < m_v \leq 30\% : \Delta\sigma_{\text{wet-dry}}^0 \leq -2.03\log(\text{NDVI}) - 0.71$$

$$m_v \geq 30\% : \Delta\sigma_{\text{wet-dry}}^0 \geq -2.03\log(\text{NDVI}) - 0.71$$

These soil moisture equations can then be used to estimate soil moisture using microwave imagery ($\Delta\sigma_{\text{wet-dry}}^0$) in wet

and dry seasons and optical imagery (NDVI) in wet season.

4. Results and discussions

With NDVI from TM imagery in wet season and $\Delta\sigma_{\text{wet-dry}}^0$ from ERS-2 imagery in wet and dry seasons, soil moisture can be estimated using the previously developed regression equations. Fig. 7 is the NDVI and $\Delta\sigma_{\text{wet-dry}}^0$ imagery derived from TM/ERS-2 pairs in summer monsoon and winter wet seasons. The dark spots are cloud/shadow areas that have been masked out in the analysis. The soil moisture maps in the study area are shown in Fig. 8. Only a few pixels have soil moisture less than or equal to 5% and therefore are not labeled. The soil moisture map in summer monsoon season (DOY257) is built upon NDVI (DOY255) and $\Delta\sigma_{257-187}^0$. In most of the study area the soil moisture is lower than 15%. Only in some isolated areas is the moisture higher than 25% (Fig. 8a). The soil moisture map in winter wet season (DOY012) is built upon NDVI (DOY015) and $\Delta\sigma_{012-082}^0$. In most of the area the moisture is higher than 15%. In areas downhill or riverside, the moisture is higher than 25% (Fig. 8b).

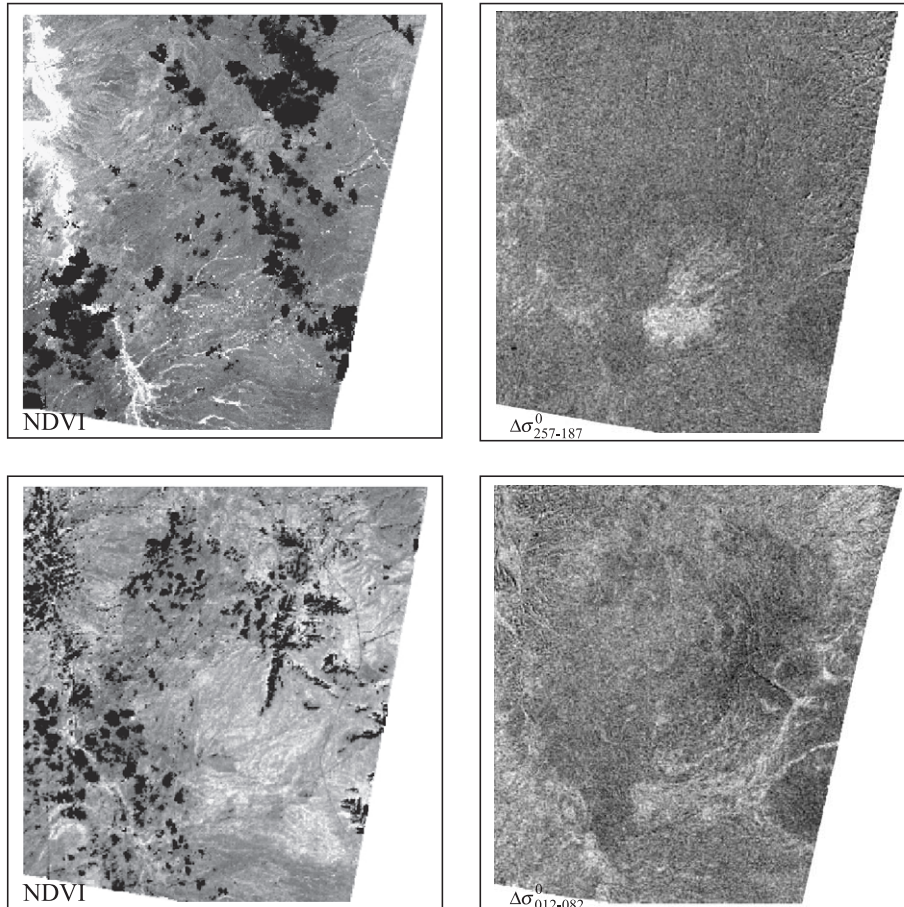


Fig. 7. NDVI and $\Delta\sigma_{\text{wet-dry}}^0$ maps in two wet seasons (summer monsoon and winter wet).

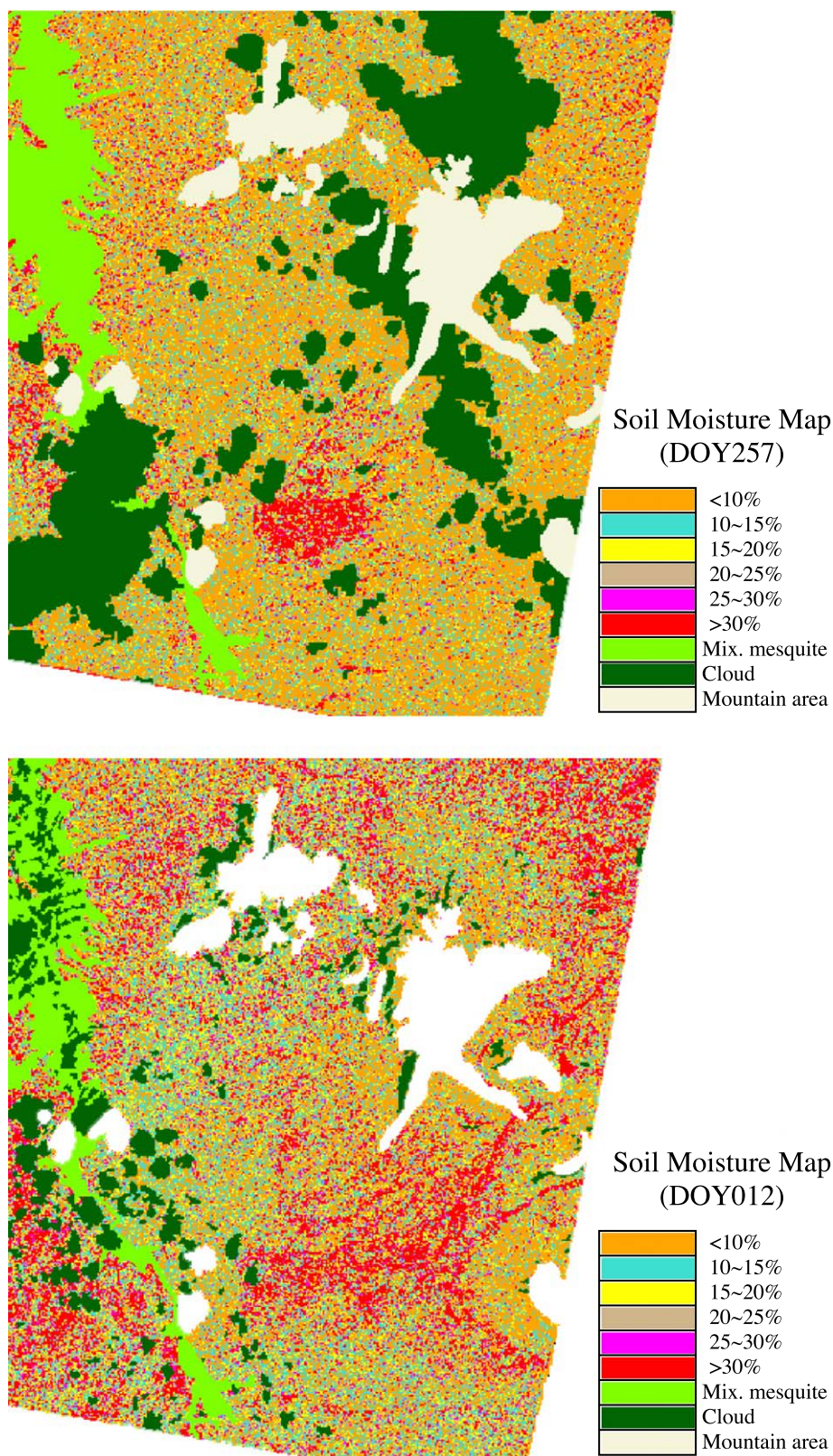


Fig. 8. Soil moisture maps in two wet seasons (summer monsoon and winter wet).

The soil moisture distribution in the study area is consistent with weather conditions in these two seasons. The precipitation is isolated short-duration thunderstorms in

summer monsoon and widespread snow or soaking rains in winter wet season. Based on the weather information (Table 1), in September 1997, a small storm occurred prior to the

ERS-2 overpass (DOY257), making some isolated areas with high soil moisture. In early January 1997, it snowed heavily and the snow had melted by the time of ERS-2 Overpass (DOY012). Thus, most of the study area, especially the alluvial fans, had high soil moisture values.

The simulated soil moisture values are also compared with ground measured soil moisture in Fig. 6b. It is shown that all sites with dry soil conditions, such as Creosote in summer monsoon (3.8%) and winter wet (9.0%), and Tobosa in summer monsoon (7.0%), are under or close to $m_v = 10\%$ isomoisture line. The measured m_v at the Sacaton site in winter wet season (28.2%) is right between the modeled 25% and 30% isomoisture lines. The measured m_v at the Tobosa site in winter wet season (19.3%) is inside the 95% confidence level of modeled 20% isomoisture line. The only problematic site is Sacaton in summer monsoon season. The measured m_v at this site is 13.8%, but it is highly above the modeled 35% isomoisture line. This inconsistency is also shown in Fig. 5. One possible reason is that the Sacaton site is in a relatively long and narrow area close to the San Pedro River. The NDVI and $\Delta\sigma_{\text{wet-dry}}^0$ may be influenced by the mixed mesquites nearby and may not represent the true value of the site where soil moisture was measured. Except the Sacaton site in summer monsoon season, the modeled soil moisture values fit the measured ones very well.

Detailed surface conditions need to be considered to further validate our results. The lower center of the

$\Delta\sigma_{257-187}^0$ image in Fig. 7 is an isolated area with a light-tone feature, indicating high $\Delta\sigma_{\text{wet-dry}}^0$ values in summer monsoon season. It is not observed in other images. The estimated soil moisture is high in both summer monsoon and winter wet seasons. We define this area as our area of interest (AOI) and detailed analysis is made over this AOI.

The AOI area was visited in April 2000. We found that it was an area with different soil texture and roughness from its adjacent areas. Although both the AOI and the adjacent areas are part of alluvial fans, the soil inside AOI is brown fine sandy loam with small portion of dispersed limestone cobbles coming from Blakeney–Luckyhills complex of fan alluvium (Soil Survey, 1996). The AOI surface is smooth with a uniform gentle slope (3–5%), while the adjacent areas are rougher with more gravel and cobbles. The vegetation conditions are a little different, too. However, from the land cover map in Fig. 1, both the AOI and adjacent areas belong to grassland. Therefore, the vegetation difference is neglected in model simulation.

Fig. 9 is the four ERS-2 images of our AOI: DOY012 (winter wet), DOY082 (spring dry), DOY 187 (end of spring dry), and DOY257 (summer monsoon). The images of the AOI in the dry seasons (DOY082, DOY187) are darker than the adjacent areas because of the dry and smoother soil. In winter wet season (DOY012), the snow melting was widespread and the soil moisture was similarly high between the AOI and the adjacent areas. Therefore, the image inside the AOI has a similar tone with adjacent

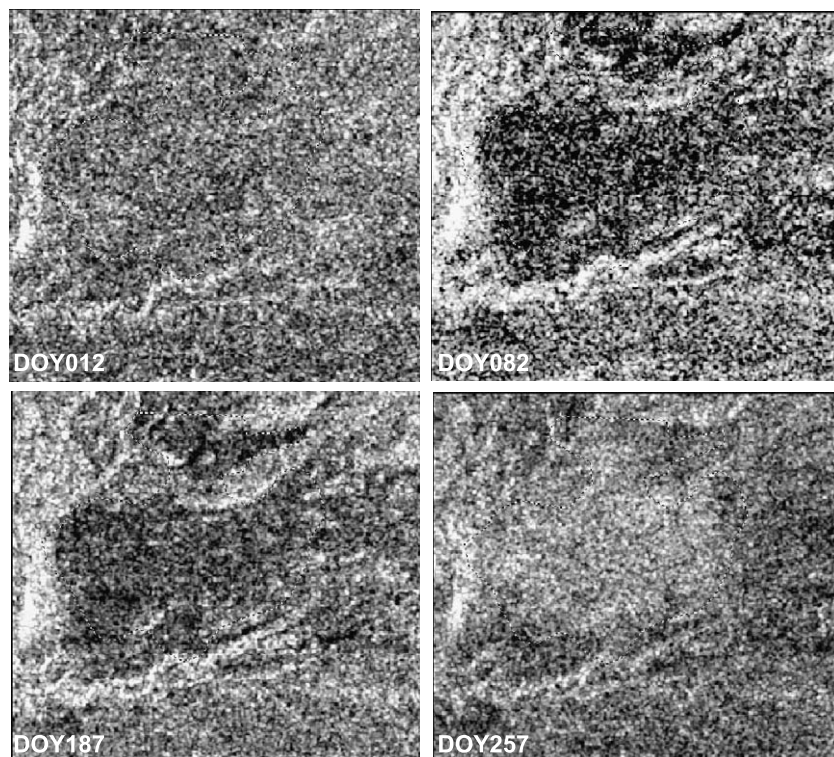


Fig. 9. Four ERS-2 σ^0 images of AOI: winter wet (DOY012), spring dry (DOY082), end of spring dry (DOY187), and summer monsoon (DOY257).

areas. In summer monsoon season (DOY257) however, the rangeland was dominated by isolated thunderstorms. An isolated thunderstorm may occur on the AOI and the adjacent areas. Because soil texture of the AOI is more capable of retaining moisture than the adjacent areas, the high backscatter inside the AOI must be related to soil moisture.

Similar conclusions can be made when the annual changes of NDVI and σ^0 are plotted for the AOI (Fig. 10a) and the adjacent areas (Fig. 10b). The NDVI change of AOI and the adjacent areas has a similar flow, indicating similar vegetation conditions. The σ^0 change however, is very different. In winter wet season, both areas are moistened by snow melting so the backscatter is similarly high (> -10 dB) in the AOI and the adjacent areas. In spring dry season, both areas are similarly dry, but SAR backscatter of the AOI is much lower than the adjacent areas because the surface of AOI is smoother. In summer monsoon season, radar backscatter of the AOI is higher than the adjacent areas (about 2.2 dB). Considering the similar vegetation conditions in both areas and smoother surface of AOI, the high backscatter must be contributed from soil moisture.

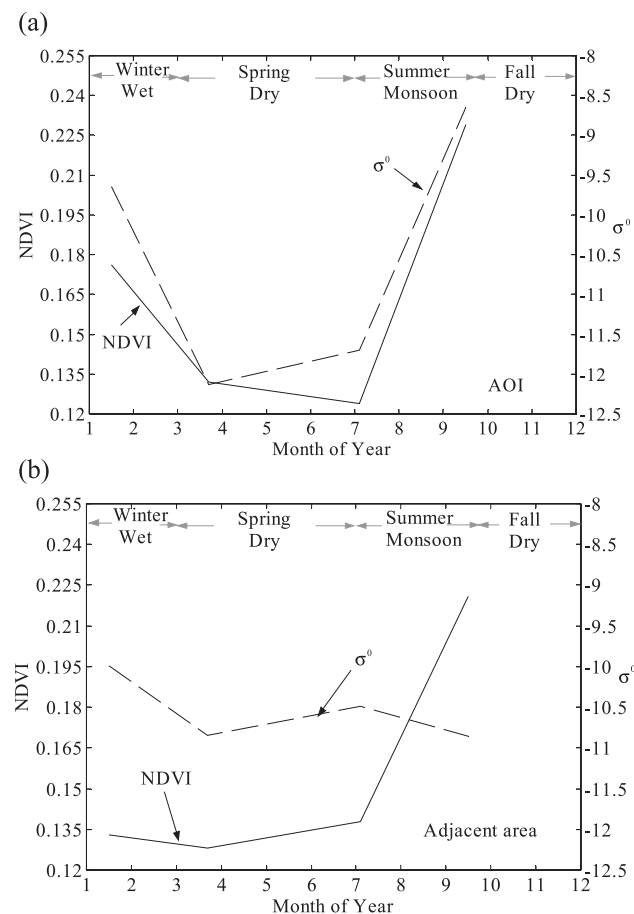


Fig. 10. Annual change of NDVI and σ^0 in 1997 for the AOI (a) and the adjacent areas (b).

5. Conclusion

An ERS-2/TM synergy to estimate soil moisture in a grass/shrub rangeland was investigated in this study. An optical/microwave synergistic model was built to simulate microwave backscattering on vegetated surfaces. Assuming there was little annual change in surface roughness in the semiarid rangelands, the effect of roughness was reduced by subtraction of two ERS-2 images between wet and dry seasons. Because NDVI values from optical TM data in wet season was almost linearly related to vegetation abundance when the vegetation density is not so high, we examined the $\Delta\sigma_{\text{wet-dry}}^0$ -NDVI relationships and built a series of isomoisture equations to estimate soil moisture in the study area.

Depending on the soil moisture contents, two $\Delta\sigma_{\text{wet-dry}}^0$ -NDVI trends were observed in the study area. When the soil surface was dry ($m_v < 10\%$), vegetation contributed more than soil in radar backscatter. Therefore, the backscatter increment from increasing vegetation exceeded the soil backscatter reduction due to vegetation attenuation. Thus, $\Delta\sigma_{\text{wet-dry}}^0$ increased with increasing NDVI. When soil moisture was higher ($m_v > 10\%$), the soil had more contribution than the vegetation. In this case, the attenuation on soil backscatter exceeded the backscatter increment from vegetation. Thus, $\Delta\sigma_{\text{wet-dry}}^0$ decreased with increasing NDVI. The trends became less obvious when vegetation density was high ($\text{NDVI} > 0.45$), in which case the dominant backscatter was from vegetation and the soil information could no longer be extracted.

The soil moisture in summer monsoon (DOY257) and winter wet (DOY012) seasons was mapped with a series of moisture intervals: $< 10\%$, $10-15\%$, $15-20\%$, $20-25\%$, $25-30\%$, and $> 30\%$. Although a thorough field validation was not possible, the soil moisture distribution was indirectly validated by examining the precipitation characteristics in each wet season. In summer monsoon season, most areas had a predominant low moisture value. Only a few isolated areas had high moisture because of the short duration thunderstorms. The moisture map in winter wet season showed a large area of high moisture value due to widespread snow melting. Further work need to be done to conduct a more thorough validation with controlled conditions.

Acknowledgements

Financial support for this paper was partially from the NASA Landsat Science Team, grant #S-41396-F at USDA-ARS Southwest Watershed Research Center, NASA's Commercial Remote Sensing Program at USDA-ARS and Michigan State University, GOFC project at Michigan State University, and USDA-ARS Global Change Research Program/SALSA program. The authors would like to thank Mr. Wanmei Ni and other colleagues

at the USDA-Agriculture Research Service, Tucson, for data processing. We would also thank Dr. Jiancheng Shi at the University of California, Santa Barbara, and Dr. Adrian Fung at the University of Texas, Arlington, who kindly provided the source of ERS-2 calibration method and the IEM model, and helped to solve many problems in model modification.

References

- Chen, K. S., Yen, S. K., & Huang, W. P. (1995). A simple model for retrieving bare soil moisture from radar-scattering coefficients. *Remote Sensing of Environment*, 54, 121–126.
- Dobson, M. C., & Ulaby, F. T. (1986). Preliminary evaluation of the SIR-B response to soil moisture, surface roughness, and crop canopy cover. *IEEE Transactions on Geoscience and Remote Sensing*, GE-24(4), 517–526.
- Dobson, M. C., & Ulaby, F. T. (1998). Mapping soil moisture distribution with imaging radar. In F. M. Henderson, & A. J. Lewis (Eds.), *Principles and applications of imaging radar, manual of remote sensing*, 3rd ed., vol. 2 (pp. 408–432). John Wiley & Sons Inc.
- Dubois, P. C., Van Zyl, J., & Engman, E. T. (1995). Measuring soil moisture with imaging radar. *IEEE Transactions on Geoscience and Remote Sensing*, 33(4), 915–926.
- Fung, A. K., Lee, Z., & Chen, K. S. (1992). Backscatter from a randomly rough dielectric surface. *IEEE Transactions on Geoscience and Remote Sensing*, 30(2), 356–369.
- Jasinski, M., & Eagleson, P. S. (1990). Estimation of subpixel vegetation cover using red-infrared scattergrams. *IEEE Transactions on Geoscience and Remote Sensing*, 28(2), 253–267.
- Karam, M. A., Fung, A. K., Lang, R. H., & Chauhan, N. S. (1992). A microwave scattering model for layered vegetation. *IEEE Transactions on Geoscience and Remote Sensing*, 30(4), 767–784.
- Moran, M. S., Bryant, R., Thome, K., Ni, W., Nouvellon, Y., Gonzalez-Dugo, M. P., Qi, J., & Clarke, T. R. (2001). A refined empirical line approach for reflectance factor retrieval from Landsat-5 TM and Landsat-7 ETM+. *Remote Sens. Environ.* 78(1–2), 71–82.
- Moran, M. S., Hymer, D. C., Qi, J., & Sano, E. (2000). Soil moisture evaluation using multi-temporal synthetic aperture radar (SAR) in semiarid rangeland. *Agricultural and Forest Meteorology*, 105, 69–80.
- Moran, M. S., Vidal, A., Troufleau, D., Qi, J., Clarke, T. R., Pinter Jr., P. J., Mitchell, T. A., Inoue, Y., & Neale, C. M. U. (1997). Combining multifrequency microwave and optical data for crop management. *Remote Sensing of Environment*, 61, 96–109.
- Oh, Y., Sarabandi, K., & Ulaby, F. T. (1992). An empirical model and an inversion technique for radar scattering from bare soil surfaces. *IEEE Transactions on Geoscience and Remote Sensing*, 30(2), 370–381.
- Qi, J., Chehbouni, A., Huete, A. R., Herr, Y., & Sorooshian, S. (1994). A modified soil adjusted vegetation index (MSAVI). *Remote Sensing of Environment*, 48, 119–126.
- Qi, J., Kerr, Y. H., Moran, M. S., Wetz, M., Huete, A. R., Sorooshian, S., & Bryant, R. (2000). Leaf area index estimates using remotely sensed data and BRDF models in a semiarid region. *Remote Sensing of Environment*, 73, 18–30.
- Sano, E. E., Huete, A. R., Troufleau, D., Moran, M. S., & Vidal, A. (1998b). Relation between ERS-1 synthetic aperture radar data and measurements of surface roughness and moisture content of rocky soils in a semiarid rangeland. *Water Resources Research*, 34(6), 1491–1498.
- Sano, E. E., Moran, M. S., Huete, A. R., & Miura, T. (1998a). C- and multiangle Ku-band synthetic aperture radar data for bare soil moisture estimation in agricultural areas. *Remote Sensing of Environment*, 64, 77–90.
- Schmullius, C. C., & Evans, D. L. (1997). Synthetic aperture radar (SAR) frequency and polarization requirements for applications in ecology, geology, hydrology, and oceanography: A tabular status quo after SIR-C/X-SAR. *International Journal of Remote Sensing*, 18(13), 2713–2722.
- Shi, J. C., Wang, J., Hsu, A. Y., O'Neil, P. E., & Engman, E. T. (1997). Estimation of bare surface soil moisture and roughness parameters using L-band SAR image data. *IEEE Transactions on Geoscience and Remote Sensing*, 35, 1254–1265.
- Soil Survey of San Pedro Valley, Arizona (1996). Interim Report, Department of the Interior Geological Survey. NRCS.
- Taconet, O., Vidal-Madjar, D., Emblanch, C., & Normand, M. (1996). Taking into account vegetation effects to estimate soil moisture from C-band radar measurements. *Remote Sensing of Environment*, 56, 52–56.
- Ulaby, F. T., Batlivala, P. P., & Dobson, M. C. (1978). Microwave backscatter dependence on surface roughness, soil moisture and soil texture: Part I. Bare soil. *IEEE Transactions on Geoscience and Remote Sensing*, 16(4), 285–295.
- Ulaby, F. T., Moore, R. K., & Fung, A. K. (1982). Microwave remote sensing: Active and passive, Vol. II, Radar remote sensing and surface scattering and emission theory. Boston: Artech House.
- Verhoest, N. E. C., Troch, P. A., Paniconi, C., & De Troch, F. P. (1998). Mapping basin scale variable source areas from multi-temporal remotely sensed observations of soil moisture behaviour. *Water Resources Research*, 34(12), 3235–3244.
- Wallace, O. C., Qi, J., Heilman, P., & Marsett, R. C. (2003). Remote sensing for cover change assessment in southeast Arizona. *Journal of Range Management*, 56, 402–409.
- Wang, Y., Kasischke, E. S., Melack, J. M., Davis, F. W., & Christensen Jr., N. L. (1994). The effects of changes in loblolly pine biomass and soil moisture on ERS-1 SAR backscatter. *Remote Sensing of Environment*, 49, 25–31.
- Wever, T., & Henkel, J. (1995). Evaluation of the AIRSAR system for soil moisture analysis. *Remote Sensing of Environment*, 53, 118–122.